

Rotating Scalar Field and Formation of Bose Stars

Kuldeep J. Purohit,^{1,*} Pravin Kumar Natwariya^{1,2,3,†}, Jitesh R. Bhatt^{1,2,‡} and Prashant K. Mehta^{1,§}

¹Physics Department, Faculty of Science, The Maharaja Sayajirao University of Baroda, Vadodra 390 002, Gujarat, India

²Physical Research Laboratory, Theoretical Physics Division, Ahmedabad, Gujarat 380 009, India

³Department of Physics, Indian Institute of Technology, Gandhinagar, Palaj, Gujarat 382 355, India

(Dated: September 28, 2021)

Abstract

We study numerical evolutions of an initial cloud of self-gravitating bosonic dark matter with finite angular momentum. It is demonstrated that the initial spinning scalar cloud can undergo a gravitational condensation to form a Bose star in the system. The results imply that the time for the gravitational condensation changes significantly in the presence of finite angular momentum. It also strongly depends on the attractive or repulsive nature of the self-interaction in the bosonic cloud. For the cases with attractive and no self-interaction, it is demonstrated that the stars formed in our study are not having any significant rotation as all the vorticity after the gravitational condensation resides outside the star formation region. But when the case of repulsive self-interaction is considered, we show that vorticity disappears around the star formation region. This might be an indication of the rotating star. Further, we study the role of angular momentum and self-interaction on density and radius of a Bose star. We also discuss our results and their consistency with the work carried out by the earlier researchers.

Keywords: Bose Stars, Star Formation, Ultra Light Dark Matter, Bose-Einstein Condensation

I. INTRODUCTION

After observation of gravitational-wave signal GW190521 by advanced LIGO/Virgo collaboration, the formation of the Bose stars have gotten much attention [1–4]. GW190521 can be a potential signal from the merger of two Bose stars [1]. About 27 percent of the total energy budget in the Universe is the unknown matter—dark matter [5]. Dark matter can be bosonic in nature for e.g. fuzzy cold dark matter [6], invisible QCD axions [7–10] etc. Some fraction of bosonic dark matter may reside in the form of Bose stars in the Universe. In the other scenarios there can be formation of primordial black holes due to gravitational instability of scalar dark-matter [11]. There are several theoretical constraints on the bosonic dark matter mass. One can find the lower bound on boson mass to be $> 1.5 \times 10^{-33}$ eV by requiring clustering between bosons within the cosmological horizon for present-day [12]. As the dark matter is gravitationally coupled to baryonic matter, its mass can be constrained to $> 1.6 \times 10^{-28}$ eV by baryon acoustic oscillations at matter-radiation equality [12]. The lower bounds on the mass of the bosonic dark matter can be found in Refs. [13–18]. Bose stars are gravitational clumps of Bose-Einstein condensate. The Bose-Einstein Condensation occurs when the thermal de Broglie wavelength, $[2\pi/(mT)]^{1/2}$, becomes larger than the mean separation between particles, $n^{-1/3}$. Therefore, one can put the upper bound on boson mass to be < 1.87 eV [19–21]. Here, n is the number density of the dark matter, m is mass and T is temperature.

There exist various analytic solutions to the Einstein-Klein-Gordon equations describing properties of a Bose star [12,

22]. Although the study of Bose stars started earlier, there is a little progress in understanding the evolution and formation of the Bose star under various physical situations, for e.g. attractive/repulsive self-interaction between dark matter particles [23, 24]. However, recently in the references [25, 26] this has come under a sharp focus. In reference [25] the authors demonstrated that how an initial configuration of a light scalar field can undergo a gravitational collapse and form a Bose star. The authors argue that their study can help in solving the missing satellite problem and shed light on Fast Radio Bursts [27], ARCADE 2 [28] and EDGES [29] observations. The role of self-interaction in the formation of Bose stars has been studied in reference [26]. Authors of the reference [30], study the formation and stability of Bose stars by considering self-interaction—both attractive and repulsive. The superfluid dark matter may also help in solving the Milky Way rotation curve, and it requires less total-baryonic mass to solve the rotation curve, which is within the current measurements. Subsequently, superfluid dark matter is also able to show strong gravitational lensing [31, 32].

From the observations, it has been evident that gravitational clouds rotate, possibly due to gravitational shearing. Therefore it is very essential to study the formation of Bose stars under such a scenario. In the present study, we intend to study the effect of angular momentum present in the initial bosonic cloud undergoing a gravitational collapse. It becomes interesting to study whether such rotating clouds eventually form a rotating Bose star or not. In the literature, there exist several studies where the authors analyzed Bose stars with finite angular momentum. Recently, the authors of the reference [33], have shown analytically that in the absence of self-interaction or finite attractive interaction Bose stars with finite angular momentum are unstable. However, the rotating Bose star configurations can be possible when the repulsive self-interaction is present. In reference [34], the authors study the stability of a rotating Bose stars in various massive scalar field models described by the Klein-Gordon equation. Here it is found

* kuldeepjrajpurohit@gmail.com

† pvn.sps@gmail.com, pravin@prl.res.in

‡ jeet@prl.res.in

§ pk.mehta-phy@msubaroda.co.in

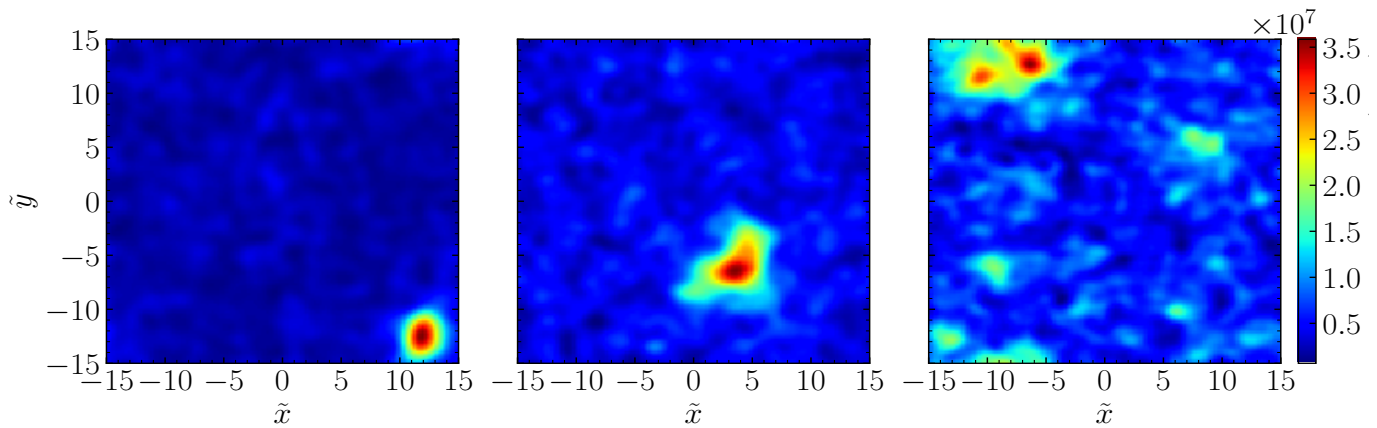


FIG. 1: Variation of Density ($|\tilde{\psi}|^2$) in the $\tilde{x}\tilde{y}$ -plane at time $\tilde{t} = 16479.5$. The total angular momentum of the system ($\tilde{\mathcal{L}}_{\text{tot}}$) varies from left to right as 0, 3, and 5. Here, we do not consider any self-interaction between particles. The box size \tilde{L} is 30 and $\tilde{N} = 10$.

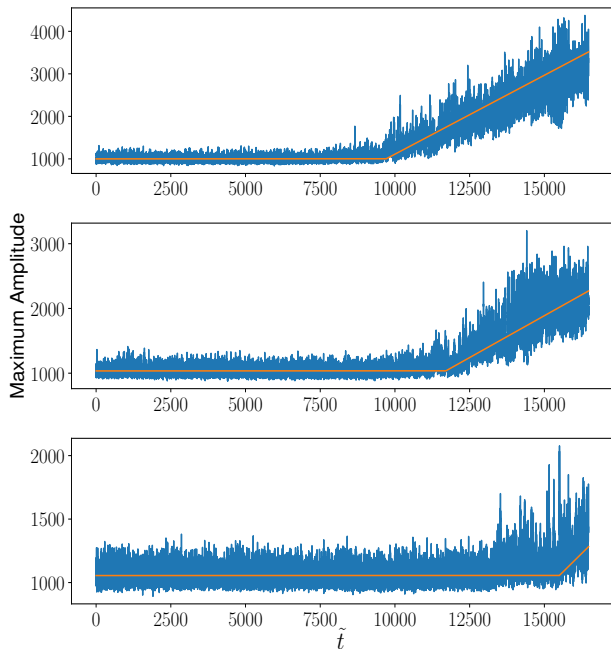


FIG. 2: Time evolution of the maximum amplitude of $|\psi|$ for different values of initial angular momentum of bosonic field for $\tilde{g} = 0$. $\tilde{\mathcal{L}}_{\text{tot}}$ varies from top to bottom as 0, 3 and 5.

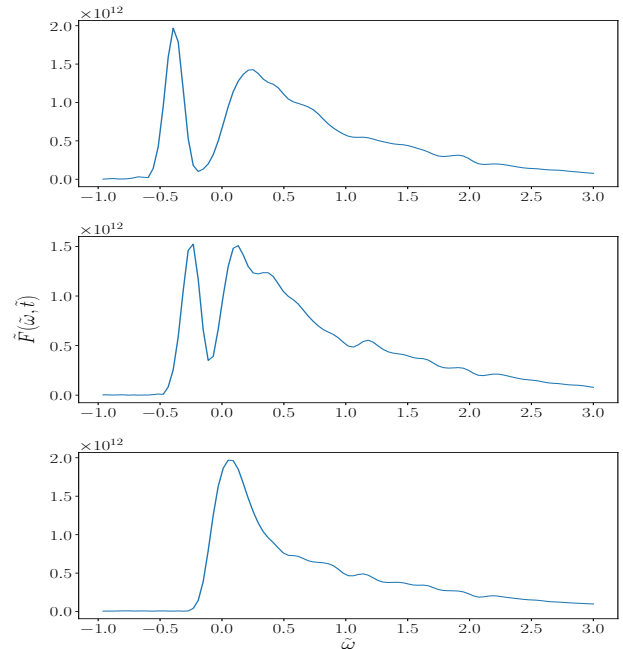


FIG. 3: Energy Spectrum, $\tilde{F}(\tilde{\omega}, \tilde{t} \sim 16479.5)$ as a function of $\tilde{\omega}$ for cases considered in figure (2). $\tilde{\mathcal{L}}_{\text{tot}}$ varies from top to bottom as 0, 3 and 5.

that mini Bose star configurations are unstable and the non-axisymmetric instability can grow exponentially. However, the instability vanishes when the growth rate ω_l is comparable to the mass of the scalar field. In the reference [35], authors consider the nonlinear Einstein Klein-Gordon and Einstein Proca systems for initially spinning axisymmetric cloud, and investigate the formation and stability of rotating Bose star under self-gravitating field. For the scalar case non-axisymmetric instability always occurs and ejects all the angular momentum from star. But for the Proca system one can find a stable configuration of the rotating star. In the present work, we intend to study the formation of a Bose star when the initial field has a finite angular momentum. The initial cloud is

considered to be dilute nonaxisymmetric but with a nonzero angular momentum. We study the evolution of such a system under the influence of its self gravity. We also analyzed the effect of the both attractive and repulsive interactions on the star formation. The presence of initial field rotation can significantly affect the star formation time for different values of angular momentum. We shall demonstrate below that the presence of angular momentum and self-interaction can strongly influence the dynamics of Bose star formation and properties of the star.

This work is divided into the following sections: In section [II], we discuss the time evolution of boson particles for various cases (attractive/repulsive self-interaction and angu-

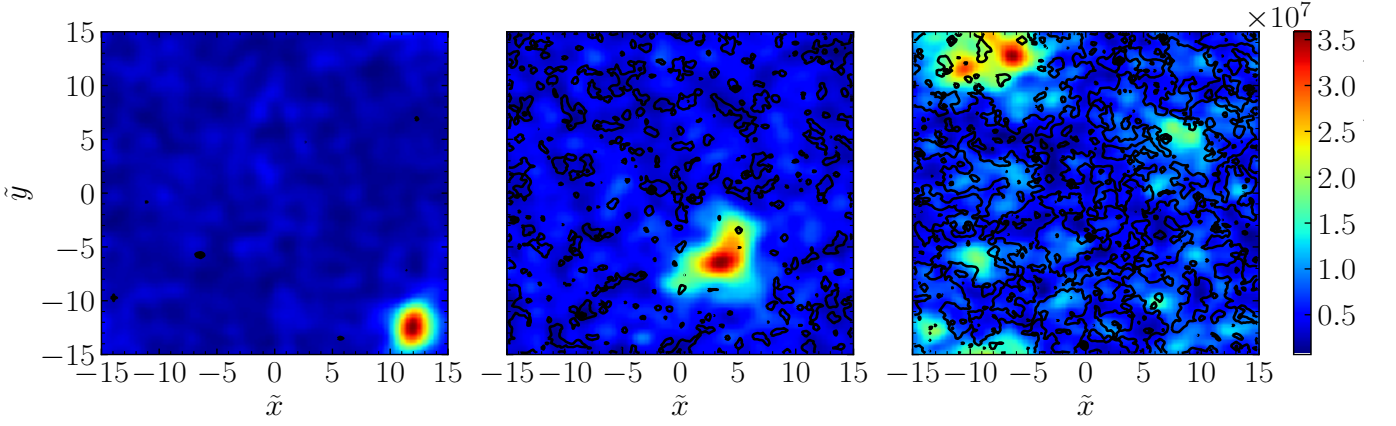


FIG. 4: Vorticity magnitude plotted in $\tilde{x}\tilde{y}$ plane at time $\tilde{t} = 16479.5$ together with the density ($|\tilde{\psi}|^2$) as shown in figure (1). The all cases shows the absence of vorticity in the star forming region.

lar momentum); in section [III], we discuss the results for above mentioned cases, and finally we conclude the results in section [IV]. Throughout the paper, we use natural units $c = k_B = \hbar = 1$. Where, c is the speed of light, k_B is the Boltzmann constant and \hbar is the reduced Planck constant. The quantities in the bold face represent the three vectors.

II. EVOLUTION OF THE BOSE STAR

In the Non-relativistic limit and for high mean occupation number, the system can be represented by a classical scalar field, $\psi(\mathbf{r}, t)$, whose time evolution can be described by the Gross-Pitaevskii-Poisson equation [23, 30, 36, 37],

$$i \frac{\partial \psi}{\partial t} = -\frac{1}{2m} \nabla^2 \psi + m \Phi \psi + g |\psi|^2 \psi, \quad (1)$$

$$\nabla^2 \Phi = 4\pi G m (|\psi|^2 - n), \quad (2)$$

where, $\Phi \equiv \Phi(\mathbf{r}, t)$ is the gravitational potential. G is universal gravitational constant and n is the mean particle density of boson gas. g is the self-interaction coupling constant, it is positive for repulsive self-interaction and negative for attractive self-interaction. $g = 0$ corresponds to non-interacting case. For a box with size L and N boson particles, $n = N/L^3$. The above equations (1) and (2), can be normalized as: $r = (1/mv_0) \tilde{r}$, $t = (1/mv_0^2) \tilde{t}$, $\Phi = v_0^2 \tilde{\Phi}$, $\psi = (v_0^2 \sqrt{m/4\pi G}) \tilde{\psi}$ and $g = (4\pi G/v_0^2) \tilde{g}$. Using $N = \int d^3r |\psi|^2$, one can get $N = (v_0/4\pi G m^2) \tilde{N}$ and it implies $n = (mv_0^4/4\pi G) \tilde{n}$. Here, v_0 is the reference velocity [30]. After normalization, the equations becomes dimensionless,

$$i \frac{\partial \tilde{\psi}}{\partial \tilde{t}} = -\frac{1}{2} \tilde{\nabla}^2 \tilde{\psi} + \tilde{\Phi} \tilde{\psi} + \tilde{g} |\tilde{\psi}|^2 \tilde{\psi}, \quad (3)$$

$$\tilde{\nabla}^2 \tilde{\Phi} = |\tilde{\psi}|^2 - \tilde{n}. \quad (4)$$

In the present work, we consider the initial rotating boson field at $\tilde{t} = 0$ as [21, 25, 33, 36–38],

$$\tilde{\psi}(\tilde{\mathbf{r}}, \tilde{t} = 0) = \tilde{N}^{1/2} \frac{1}{\pi^{3/4}} e^{-\tilde{r}^2/2} e^{i l \tan^{-1}(\tilde{y}/\tilde{x})}, \quad (5)$$

Here, we take $\tilde{N} = 10$ and box size $\tilde{L} = \tilde{L}_x = \tilde{L}_y = \tilde{L}_z = 30$. Parameter l helps in controlling the total angular momentum of the system, $\tilde{\mathcal{L}}_{\text{tot}}$. To get the initial distribution of bosons in the momentum space, we find the Fourier transform of $\tilde{\psi}(\tilde{\mathbf{r}}, \tilde{t} = 0)$. Then multiply the Fourier transform with random phase $e^{i A_p}$ to get the initial momentum distribution in the box [25, 39]. Here A_p is randomly distributed between 0 to 2π . To analyse the Bose star formation for initial rotating field, we use the publicly available code `AxioNyx` [40] with necessary modifications [41, 42]. For the present work, we fix the resolution of the box to 128^3 . The reduced total angular momentum of field in x , y and z directions can be defined by stress-energy tensor [43]. The stress-energy tensor can be written as

$$\tilde{T}^{0i} = \frac{i}{2} (\tilde{\psi} \tilde{\partial}_i \tilde{\psi}^* - \tilde{\psi}^* \tilde{\partial}_i \tilde{\psi}). \quad (6)$$

The total angular momentum in \tilde{x} , \tilde{y} and \tilde{z} direction in term of stress-energy tensor can be defined as [43],

$$\tilde{J}^i = \int (\tilde{x}^j \tilde{T}^{j0} - \tilde{x}^j \tilde{T}^{i0}) d^3 \tilde{x}. \quad (7)$$

For considered initial distribution in equation (5), the total angular momentum in \tilde{x} and \tilde{y} direction (\tilde{J}^{23} and \tilde{J}^{31} respectively) are zero. Therefore, one gets the total angular momentum of the system to be $\tilde{\mathcal{L}}_{\text{tot}} = \tilde{J}^{12} = l \tilde{N}$. To find the vorticity for the system, we introduce the “velocity”, $\mathbf{v} = \mathcal{J}/\rho$. Here, \mathcal{J} represents the current density and $\rho = |\psi|^2$. Current density \mathcal{J} is defined from equation (1) as $\mathcal{J} = i/2 (\psi \nabla \psi^* - \psi^* \nabla \psi)$. From these we can now introduce the vorticity $\boldsymbol{\Omega} = \nabla \times \mathbf{v}$.

First, we note that in our numerical results when there is no net angular momentum, the star formation can occur when the self-interaction parameter $|g|$ have a maximum value around $\sim 10^{-8}$. For values of $|g|$ higher than this we do not get the star formation. Therefore, in the present work we have considered $|g| = 10^{-8}$ for the both attractive and repulsive self-interactions. Further, we take three values of angular momentum, i.e., $\tilde{\mathcal{L}}_{\text{tot}} = 0, 3, \& 5$ and study the formation of star.

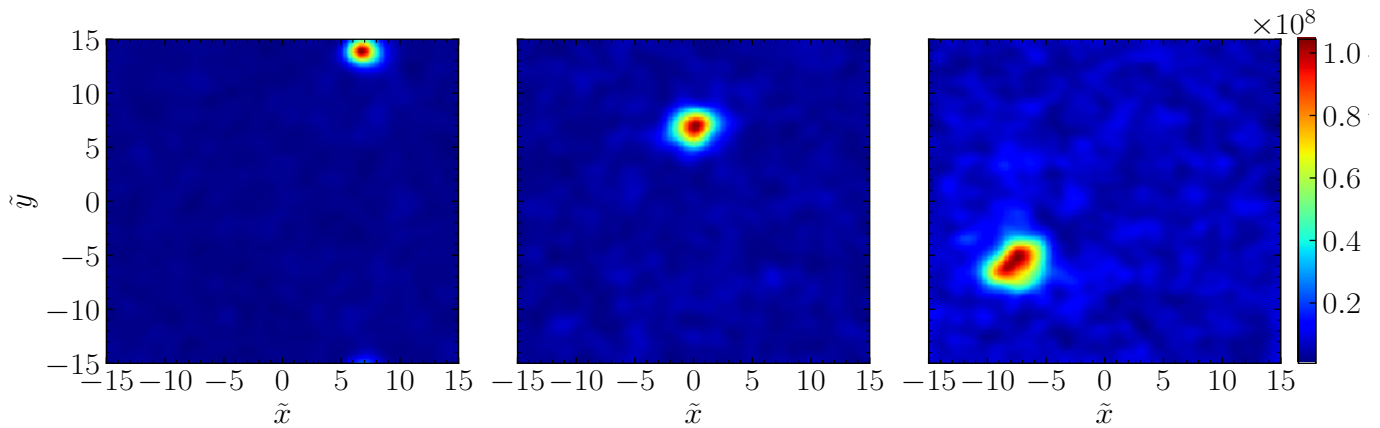


FIG. 5: The caption is same as considered in figure (1) except there is attractive self-interaction between particles ($\tilde{g} = -10^{-8}$).

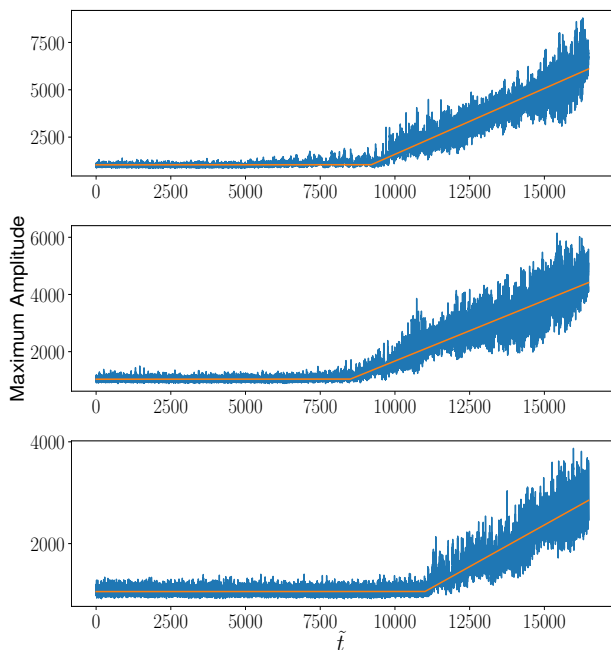


FIG. 6: The caption is same as considered in figure (1) except there is attractive self-interaction between particles ($\tilde{g} = -10^{-8}$).

III. RESULTS AND DISCUSSION

To get time evolution of initial rotating bosonic field under self-gravity, we solve the coupled non-linear equations (3) and (4) using the AxioNyx code [41, 42] with necessary modifications. For analyzing the data, we have used The yt Project [44] [45]. In order to check that the star formation has indeed happened in our numerical results, we employ the following two checks:

i) First one is to study time evolution of the maximum amplitude $|\psi(\tilde{x}, \tilde{t})|$. When the condensation of the matter occurs, there is a sudden increase in the maximum amplitude at time

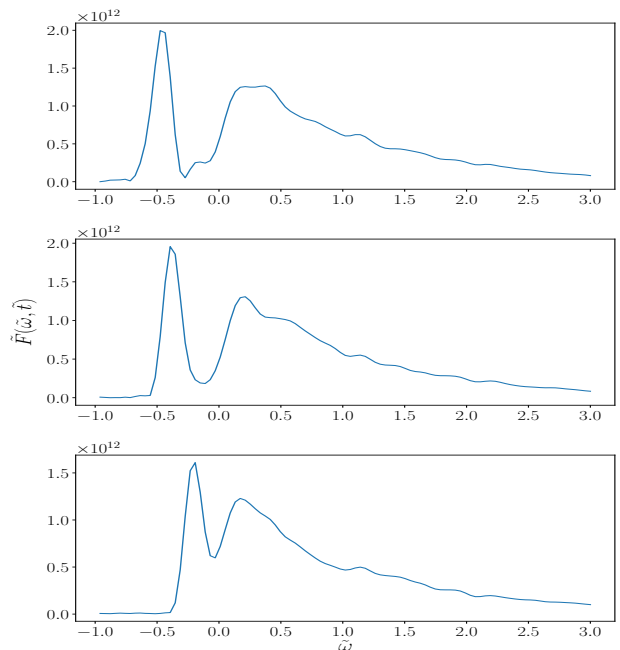


FIG. 7: The caption is same as considered in figure (1) except there is attractive self-interaction between particles ($\tilde{g} = -10^{-8}$).

τ_{gr} . The value of τ_{gr} can be estimated as [25],

$$\tau_{gr} = \frac{b\sqrt{2}}{12\pi^3} \frac{mv_0^6}{G^2 n^2 \Lambda}, \quad (8)$$

where, $b \sim 1$, $\Lambda = \log(mv_0 L)$, and n is the boson number density.

ii) Next check is to study the Energy spectrum $F(t, \omega)$, as [25],

$$F(\omega, t) = \int \frac{dt_1}{2\pi} d^3\mathbf{x} \psi^*(t, \mathbf{x}) \psi(t + t_1, \mathbf{x}) e^{i\omega t_1 - t_1^2/\tau_1^2} \quad (9)$$

is valid in the kinetic regime $1/(mv_0^2) \ll \tau_1 \ll \tau_{gr}$. Around the time when the gravitational condensation happens, $F(\omega, t)$

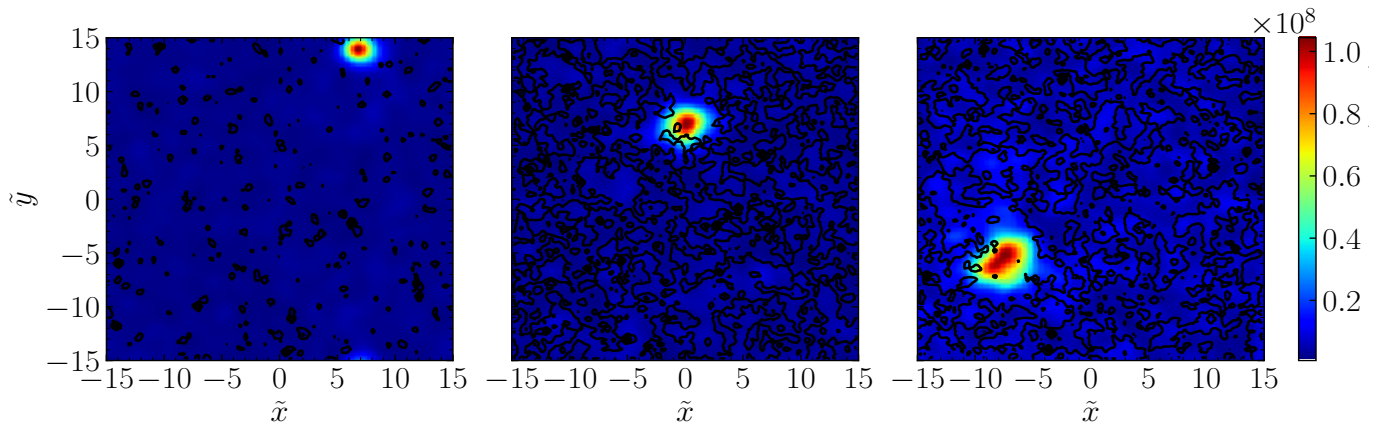


FIG. 8: Vorticity magnitude plotted in $\tilde{x}\tilde{y}$ plane at time $\tilde{t} = 16479.5$ together with the density ($|\tilde{\psi}|^2$) as shown in figure (5). The all cases shows the absence of vorticity in the star forming region.

starts developing a peak at $\omega_s < 0$ which indicates the formation of a gravitationally bound state. To make dimensionless $F(t, \omega)$, we multiply it by mv_0^2/N , i.e. $\tilde{F} = (mv_0^2/N)F$ and we can define a dimensionless measure of the Energy $\tilde{\omega} = (1/mv_0^2)\omega$.

A. Bose star formation without any self-interaction

We estimate the gravitational condensation time $\tilde{\tau}_{gr} \sim 9976$ for $\tilde{N} = 10$, $\tilde{L} = 30$ and $b = 1.2$ using equation (8). Here, it is to be noted that, equation (8) is derived in absence of angular momentum. For the cases with finite angular momentum $\tilde{\tau}_{gr}$ value will differ significantly from equation (8).

In figure (1) we have shown the snapshot of density $|\tilde{\psi}|^2$ in $\tilde{x}\tilde{y}$ -plane at time $\tilde{t} = 16479.5$. The colour bar indicates variation in $|\tilde{\psi}|^2$. The plots from the left to right respectively correspond the case with total angular momentum $\tilde{L}_{tot} = 0, 3$ and 5.

In figure (2) we have shown the evolution of maximum amplitude $|\tilde{\psi}|$ upto time $\tilde{t} = 16479.5$. The plots from the top to bottom respectively correspond the case with total angular momentum $\tilde{L}_{tot} = 0, 3$ and 5. It can be seen that for $\tilde{L}_{tot} = 0$, $\tilde{\tau}_{gr} \sim 9700$, which is in well agreement with the analytical result. Similar is the case with $\tilde{L}_{tot} = 3$. But for $\tilde{L}_{tot} = 5$ there is a very slight increase in the maximum amplitude at $\tilde{t} \sim 15500$.

In figure (3) we have shown the Energy spectrum, $\tilde{F}(\tilde{\omega})$ versus $\tilde{\omega}$ at time $\tilde{t} \sim 16479.5$. The plots from the top to bottom respectively correspond the case with total angular momentum $\tilde{L}_{tot} = 0, 3$ and 5. For $\tilde{L}_{tot} = 0$ & 3, it can be seen that a peak at $\tilde{\omega} < 0$ which indicates that Bose star nucleation has begun. In the case of $\tilde{L}_{tot} = 5$, a peak at $\tilde{\omega} < 0$ is not observed indicating that the process of Bose star nucleation has not yet begun.

For the case with zero angular momentum and no self-interaction, we have found $\tilde{\tau}_{gr} \sim 9700$, so we have kept the upper bound on time at $\tilde{t} \lesssim 16500$ for the no self-interaction case due to computational limitations. For the cases where the star is not formed even at $\tilde{t} \sim 16500$, we cannot rule out the possibility that the star will not form at later times too, but

we have demonstrated that the presence of angular momentum and self-interaction in the initial field can significantly affect the properties of star such as, its central density, mass, radius and condensation time.

Now the question is to find out if we study the gravitational collapse in a rotating initial cloud, then how much intrinsic angular momentum the Bose star can have? To get the answer to this question we plot in figure (4) vorticity magnitude distribution in the $\tilde{x}\tilde{y}$ -plane along with density plots shown in figure (1) at time $\tilde{t} = 16479.5$. The figure shows that there is no vorticity is present in the regions where the Bose star is situated. Thus our analysis indicate that though our initial cloud had finite angular momentum, but the star that is getting formed does not have any angular momentum. Similar kind of behavior was seen in [35] while studying numerical solutions of nonlinear Einstein-Klein-Gordon system. However, in this study no self-interaction of Klein-Gordon field was taken into account. Further, we also note that, in reference [33], it was demonstrated that the Bose star with finite angular momentum are unstable. Our results also consistent with the above analytical assertion.

B. Bose star formation in presence of self-interaction

Next we study Bose star formation in presence of the finite self-interaction. Our results show that the star formation occurs only when the self-interaction parameter satisfy the condition $|\tilde{g}| \lesssim 10^{-8}$. As we lower $|\tilde{g}|$ much below this limit, our results approaches the case when there is no self-interaction. Thus, in this section we shall focus on the maximum allowed value of $|\tilde{g}| = 10^{-8}$. In this section we discuss both the cases of attractive ($\tilde{g} < 0$) and repulsive ($\tilde{g} > 0$) self-interactions.

1. Attractive self-interaction

Here we discuss results of star formation when there is an attractive self-interaction $\tilde{g} = -10^{-8}$. It can be seen from (5) & (6) that star indeed forms in all the three cases. So, one can

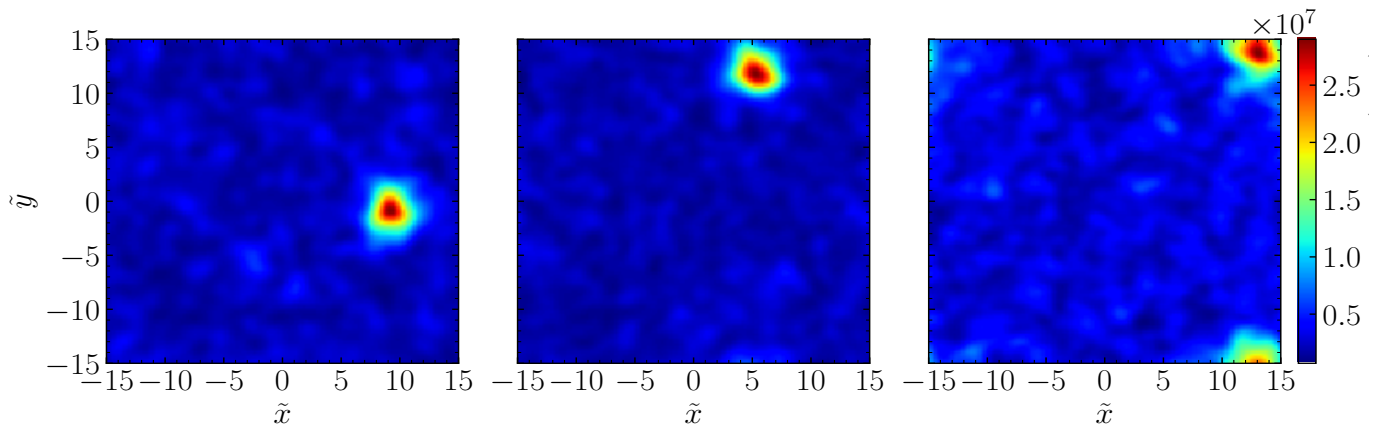


FIG. 9: Variation of Density ($|\tilde{\psi}|^2$) for the repulsive self-interaction between particles ($\tilde{g} = 10^{-8}$) in the $\tilde{x}\tilde{y}$ -plane at times $\tilde{t} = 16479.5$ for left and 27465.7 for middle and right figures. The total angular momentum of the system ($\tilde{\mathcal{L}}_{\text{tot}}$) varies from left to right as 0, 3, and 5. The box size \tilde{L} is 30 and $\tilde{N} = 10$.

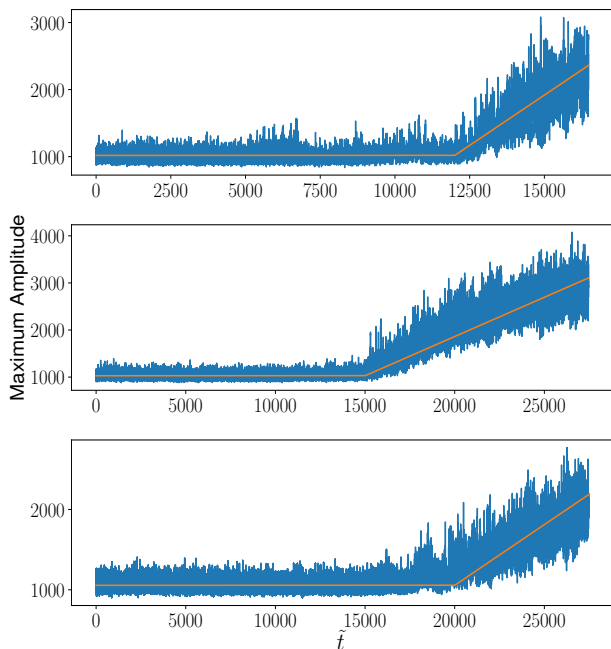


FIG. 10: The caption is same as considered in figure (2) except there is a repulsive self-interaction between particles ($\tilde{g} = 10^{-8}$).

argue that attractive self-interaction promotes star formation and works along with gravitational pressure against Heisenberg's uncertainty pressure. Here also it can be seen that as the angular momentum of the initial field increases, the central density, radius, and mass of the star decreases.

In figure (8), we have plotted vorticity magnitude on density to check whether the star has got any intrinsic angular momentum, but it can be seen that there is no vorticity present inside the star, implying absence of intrinsic angular momentum.

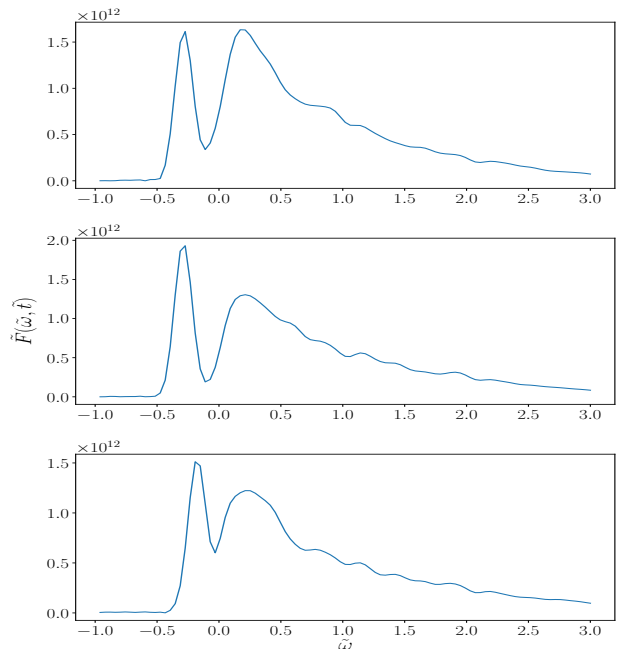


FIG. 11: Energy Spectrum, $\tilde{F}(\tilde{\omega}, \tilde{t})$ as a function of $\tilde{\omega}$ at times $\tilde{t} \sim 16479.5$ (upper) and 27465.7 (middle and lower). $\tilde{\mathcal{L}}_{\text{tot}}$ varies from top to bottom as 0, 3 and 5. Here, we have considered the repulsive self-interaction between particles ($\tilde{g} = 10^{-8}$).

2. Repulsive self-interaction

In figure (9), we have shown the snapshot of density profile at $\tilde{t} = 16479.5$ (left figure) and $\tilde{t} = 27465.7$ (middle and right figures). For the repulsive self-interaction, star formation time increases significantly when we increase the angular momentum as shown in the figure (10). In figure (10), one can see that for $\tilde{\mathcal{L}}_{\text{tot}} = 0$ case, the star formation begins at $\tilde{t}_{gr} \sim 12000$; whereas for $\tilde{\mathcal{L}}_{\text{tot}} = 3$ case, the star formation be-

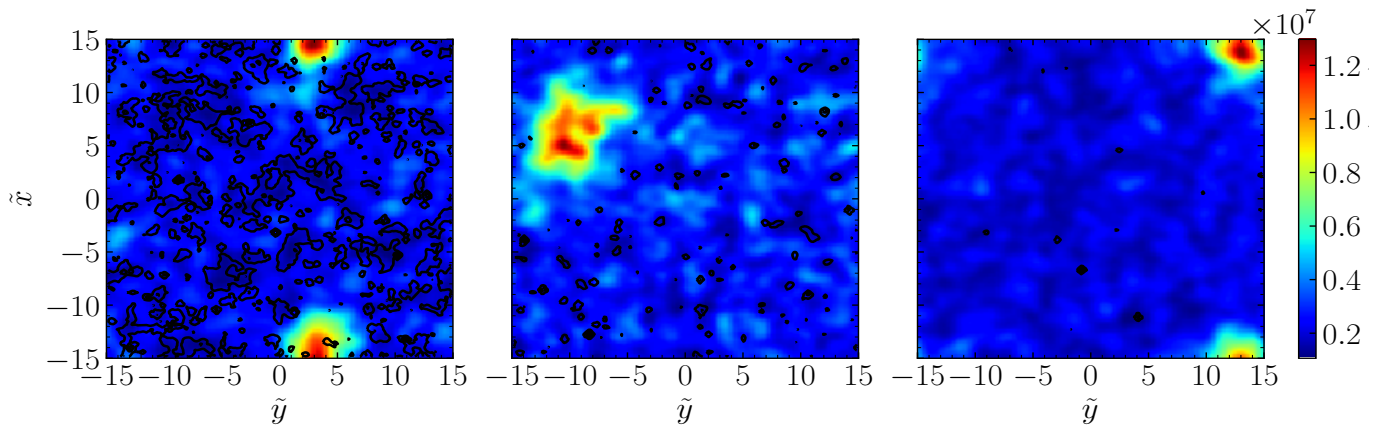


FIG. 12: Vorticity magnitude plotted in $\tilde{x}\tilde{y}$ plane at times $\tilde{t} = 21972.6, 23345.9$ and 27465.7 from left to right together with the density ($|\tilde{\psi}|^2$) for $\tilde{g} = 10^{-8}$ (repulsive self-interaction) and $\tilde{\mathcal{L}}_{\text{tot}} = 5$. With the passage of time the net vorticity vanishes from the surrounding of the star formation region.

gins at $\tilde{\tau}_{gr} \sim 15000$; and for $\tilde{\mathcal{L}}_{\text{tot}} = 5$ case, the star formation begins at $\tilde{\tau}_{gr} \sim 20000$. It is to be noted that the star formation time compared to no self-interaction case has increased, this is expected since the repulsive self-interaction acts as an extra pressure along with Heisenberg's uncertainty pressure against gravity which will eventually hinder the star formation process. Next by increasing angular momentum from zero it further increases the star formation time $\tilde{\tau}_{gr}$. From (10) it can be seen that the process of star formation have not begun till $\tilde{t} = 16479.5$ for $\tilde{\mathcal{L}}_{\text{tot}} = 3$ & 5.

To check the evolution of the initial angular momentum in the box we have plotted vorticity magnitude. In figure (12) plots of vorticity magnitude and $|\tilde{\psi}|^2$ in $\tilde{x}\tilde{y}$ plane for the total angular momentum $\tilde{\mathcal{L}}_{\text{tot}} = 5$ are shown for three different times $\tilde{t} = 21972.6, 23345.9$ and 27465.7 from the left to right. For $\tilde{\mathcal{L}}_{\text{tot}} = 5$ value of $\tilde{\tau}_{gr}$ is $\sim 2 \times 10^4$. As we see from the figure for $\tilde{t} \gg \tilde{\tau}_{gr}$, surprisingly we observe that there is no vorticity in the plane. We have also checked the absence of vorticity in $\tilde{x}\tilde{z}$ and $\tilde{y}\tilde{z}$ planes. It is possible that vorticity might have entered the star formation region. But due to strong density fluctuations in this region, it not possible to study net angular momentum of the star. This is consistent with the stability analysis carried in Ref. [33], where it is reported to have a stable Bose star with finite angular momentum. We have also varied values of $\tilde{\mathcal{L}}_{\text{tot}}$ and found that for $\tilde{t} \gg \tilde{\tau}_{gr}$, vorticity vanishes in the box.

In figure (13a), we show the effect of self-interaction on density of the Bose star. In this plot, we consider $\tilde{\mathcal{L}}_{\text{tot}} = 0$. It can be seen that for attractive self-interaction the star is much dense and compact as compared to no and repulsive self-interaction. We have summarized the numerical data in Table (I). Similar pattern can also be seen for the case with no self-interaction. In figure (13b), we show the effect of angular momentum on density of the Bose star. However, figure (13a) shows that under the influence of attractive self-interaction the central density can be higher than the no interaction case whereas the central density can be lower in comparison for the repulsive interaction. In figures (13b) and (13c), density versus radius plots are shown at equal time and "equal" masses

respectively for different values of total angular momentum. In plot (13c), as we increase the angular momentum from 0 (blue curve) to 3 (orange curve) and 5 (green curve), the time for same-density star formation increases from $\tilde{t} = 10701.5, 13448.1$ and 16479.5 , respectively. This indicates that the presence of finite angular momentum does not significantly alter the mass and radius of Bose stars from the zero angular momentum case with attractive self-interaction. Similar patterns can be seen in the case when there is no self-interaction. We have summarized the numerical data in Table (II). Similar pattern can also be seen for the case with no self-interaction. In the tables (I) and (II), R_{95} represents the radius of the star that encloses the 95 percent density of Bose star.

TABLE I: Central density and radius corresponding to Bose star shown in Figure (13a) at time $\tilde{t} = 16479.5$. All the numbers are dimensionless in the rescaled units as defined in the main text.

	Central Density	R_{95}
Attractive Self-Interaction	4.56×10^7	2.2
No Self-Interaction	1.10×10^7	3.3
Repulsive Self-Interaction	7.44×10^6	4.0

TABLE II: Central density and radius corresponding to Bose star shown in Figure (13b) at time $\tilde{t} = 16479.5$. All the numbers are dimensionless in the rescaled units as defined in the main text.

	Central Density	R_{95}
$\tilde{\mathcal{L}}_{\text{tot}} = 0.0$	4.56×10^7	2.2
$\tilde{\mathcal{L}}_{\text{tot}} = 0.3$	1.75×10^7	3.0
$\tilde{\mathcal{L}}_{\text{tot}} = 0.5$	5.70×10^6	4.3

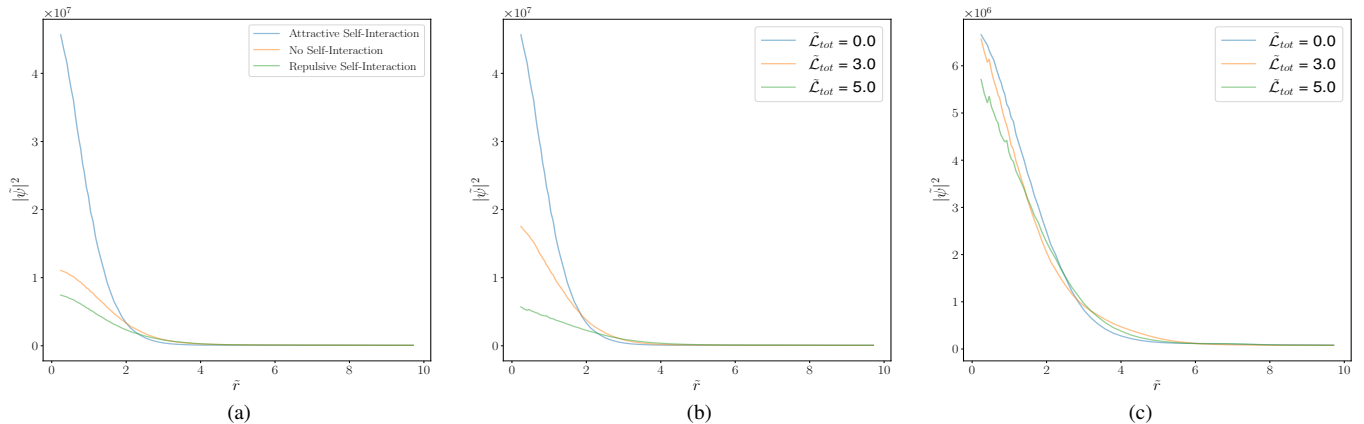


FIG. 13: **(a)** Density profiles of Bose star as a function of distance from center of star for no self-interaction, attractive and repulsive self-interaction at time $\tilde{t} = 16479.5$ when there is no angular momentum. **(b)** Density profiles of Bose star as a function of distance from center of star for attractive self-interaction at time $\tilde{t} = 16479.5$. Here we consider three cases: $\tilde{\mathcal{L}}_{\text{tot}} = 0, 3$ and 5 . **(c)** Density profiles of Bose star as a function of distance from center of star for attractive self-interaction at different times. We consider three cases with total angular momentum $\tilde{\mathcal{L}}_{\text{tot}} = 0, 3$ and 5 at times $\tilde{t} = 10701.5, 13448.1$ and 16479.5 , respectively. To get nearly same density-radius profile one needs to increase the star evolution time as angular momentum increases.

IV. CONCLUSIONS

We have analyzed the role of angular momentum in the initial boson cloud with the self-gravitation that can affect the formation of a Bose star. It is known in the literature that Bose stars made of a complex scalar field with the total angular momentum $\neq 0$ are unstable either in the case of attractive or negligibly small self-interactions [33]. In this work we have considered the initial bosonic cloud with having finite angular momentum. In this condition also for negligible and attractive self-interaction cases, we show that the star formation is possible. Our plots of vorticity magnitude show that there is hardly any vorticity in the star forming region, implying that the stars produced under the above conditions may not have a significant angular momentum. Surprisingly for the case of

repulsive interaction, our analysis show the absence of vorticity outside the star formation region. This could be a possible indication of formation of a rotating star.

V. ACKNOWLEDGMENTS

We are grateful to Bodo Schwabe and Mateja Gosenca for helpful discussions and helping with the publicly available code `AxiONyx`. The authors would also like to thank Profs. Dmitry G. Levkov and Dilip Angom for the valuable suggestions. All the computations are accomplished on the Vikram-100 HPC cluster at Physical Research Laboratory, Ahmedabad.

-
- [1] J. C. Bustillo, N. Sanchis-Gual, A. Torres-Forné, J. A. Font, A. Vajpeyi, R. Smith, C. Herdeiro, E. Radu, and S. H. Leong, *Physical Review Letters* **126** (2021), 10.1103/physrevlett.126.081101.
 - [2] R. Abbott, T. Abbott, S. Abraham, F. Acernese, K. Ackley, C. Adams, R. Adhikari, V. Adya, C. Affeldt, M. Agathos, and et al., *Physical Review Letters* **125** (2020), 10.1103/physrevlett.125.101102.
 - [3] J. Aasi, B. P. Abbott, R. Abbott, T. Abbott, M. R. Abernathy, K. Ackley, C. Adams, T. Adams, P. Addesso, and et al., *Classical and Quantum Gravity* **32**, 074001 (2015).
 - [4] F. Acernese, M. Agathos, K. Agatsuma, D. Aisa, N. Allemandou, A. Allocca, J. Amarni, P. Astone, G. Balestri, G. Ballardín, and et al., *Classical and Quantum Gravity* **32**, 024001 (2014).
 - [5] N. Aghanim, Y. Akrami, M. Ashdown, J. Aumont, C. Baccigalupi, M. Ballardini, A. J. Banday, R. B. Barreiro, N. Bartolo, and et al., *Astronomy & Astrophysics* **641**, A6 (2020).
 - [6] W. Hu, R. Barkana, and A. Gruzinov, *Phys. Rev. Lett.* **85**, 1158 (2000).
 - [7] J. Preskill, M. B. Wise, and F. Wilczek, *Physics Letters B* **120**, 127 (1983).
 - [8] E. W. Kolb and I. I. Tkachev, *Physical Review Letters* **71**, 3051–3054 (1993).
 - [9] M. S. Turner, *Phys. Rev. D* **33**, 889 (1986).
 - [10] C. Hogan and M. Rees, *Physics Letters B* **205**, 228 (1988).
 - [11] M. Y. Khlopov, B. A. Malomed, and Y. B. Zel'dovich, *Monthly Notices of the Royal Astronomical Society* **215**, 575 (1985), <https://academic.oup.com/mnras/article-pdf/215/4/575/4082842/mnras215-0575.pdf>.
 - [12] D. J. E. Marsh and S. Hoof, “Astrophysical searches and constraints on ultralight bosonic dark matter,” (2021), [arXiv:2106.08797 \[hep-ph\]](https://arxiv.org/abs/2106.08797).
 - [13] E. Armengaud, N. Palanque-Delabrouille, C. Yèche, D. J. E. Marsh, and J. Baur, *Monthly Notices of the Royal Astronomical Society* **507**, 1000 (2021).

- cal Society **471**, 4606–4614 (2017).
- [14] H.-Y. Schive, T. Chiueh, T. Broadhurst, and K.-W. Huang, *The Astrophysical Journal* **818**, 89 (2016).
- [15] B. Bozek, D. J. E. Marsh, J. Silk, and R. F. G. Wyse, *Monthly Notices of the Royal Astronomical Society* **450**, 209–222 (2015).
- [16] P. Corasaniti, S. Agarwal, D. Marsh, and S. Das, *Physical Review D* **95** (2017), 10.1103/physrevd.95.083512.
- [17] B. V. Church, P. Mocz, and J. P. Ostriker, *Monthly Notices of the Royal Astronomical Society* **485**, 2861–2876 (2019).
- [18] V. Iršič, M. Viel, M. G. Haehnelt, J. S. Bolton, and G. D. Becker, *Physical Review Letters* **119** (2017), 10.1103/physrevlett.119.031302.
- [19] T. Fukuyama, M. Morikawa, and T. Tatakawa, *Journal of Cosmology and Astroparticle Physics* **2008**, 033 (2008).
- [20] C. G. Böhrer and T. Harko, *Foundations of Physics* **38**, 216–227 (2007).
- [21] P.-H. Chavanis, *Physical Review D* **84** (2011), 10.1103/physrevd.84.043531.
- [22] R. RUFFINI and S. BONAZZOLA, *Phys. Rev.* **187**, 1767 (1969).
- [23] J. Eby, C. Kouvaris, N. G. Nielsen, and L. C. R. Wijewardhana, *Journal of High Energy Physics* **2016** (2016), 10.1007/jhep02(2016)028.
- [24] M. S. Madsen and A. R. Liddle, *Physics Letters B* **251**, 507 (1990).
- [25] D. Levkov, A. Panin, and I. Tkachev, *Physical Review Letters* **121** (2018), 10.1103/physrevlett.121.151301.
- [26] J. Veltmaat, J. C. Niemeyer, and B. Schwabe, *Physical Review D* **98** (2018), 10.1103/physrevd.98.043509.
- [27] I. I. Tkachev, *JETP Lett.* **101**, 1 (2015), arXiv:1411.3900 [astro-ph.HE].
- [28] D. J. Fixsen, A. Kogut, S. Levin, M. Limon, P. Lubin, P. Mirel, M. Seiffert, J. Singal, E. Wollack, T. Villela, and C. A. Wuensche, *Astrophys. J.* **734**, 5 (2011).
- [29] J. D. Bowman, A. E. E. Rogers, R. A. Monsalve, T. J. Mozdzen, and N. Mahesh, *Nature* **555**, 67 (2018).
- [30] J. Chen, X. Du, E. W. Lentz, D. J. E. Marsh, and J. C. Niemeyer, “New insights into the formation and growth of boson stars in dark matter halos,” (2021), arXiv:2011.01333 [astro-ph.CO].
- [31] S. Hossenfelder and T. Mistele, *Journal of Cosmology and Astroparticle Physics* **2019**, 001–001 (2019).
- [32] S. Hossenfelder and T. Mistele, *Monthly Notices of the Royal Astronomical Society* **498**, 3484–3491 (2020).
- [33] A. Dmitriev, D. Levkov, A. Panin, E. Pushnaya, and I. Tkachev, *Physical Review D* **104** (2021), 10.1103/physrevd.104.023504.
- [34] N. Siemonsen and W. E. East, *Physical Review D* **103** (2021), 10.1103/physrevd.103.044022.
- [35] N. Sanchis-Gual, F. Di Giovanni, M. Zilhão, C. Herdeiro, P. Cerdá-Durán, J. Font, and E. Radu, *Physical Review Letters* **123** (2019), 10.1103/physrevlett.123.221101.
- [36] P.-H. Chavanis and L. Delfini, *Physical Review D* **84** (2011), 10.1103/physrevd.84.043532.
- [37] C. G. Böhrer and T. Harko, *Journal of Cosmology and Astroparticle Physics* **2007**, 025–025 (2007).
- [38] F. Guzmán, F. Lora-Clavijo, J. González-Avilés, and F. Rivera-Paleo, *Journal of Cosmology and Astroparticle Physics* **2013**, 034–034 (2013).
- [39] D. Levkov, A. Panin, and I. Tkachev, *Physical Review Letters* **118** (2017), 10.1103/physrevlett.118.011301.
- [40] <https://github.com/axionyx>.
- [41] B. Schwabe, M. Gosenca, C. Behrens, J. C. Niemeyer, and R. Easther, *Physical Review D* **102** (2020), 10.1103/physrevd.102.083518.
- [42] A. S. Almgren, J. B. Bell, M. J. Lijewski, Z. Lukić, and E. Van Andel, *The Astrophysical Journal* **765**, 39 (2013).
- [43] S. Weinberg, *Gravitation and Cosmology: Principles and Applications of the General Theory of Relativity* (Wiley, 1972).
- [44] <https://yt-project.org/doc>.
- [45] M. J. Turk, B. D. Smith, J. S. Oishi, S. Skory, S. W. Skillman, T. Abel, and M. L. Norman, *The Astrophysical Journal Supplement Series* **192**, 9 (2010).